OPTIMAL CONTROL APPLICATIONS AND METHODS
Optim. Control Appl. Meth. 0000; **00**:1–30
Published online in Wiley InterScience (www.interscience.wiley.com). DOI: 10.1002/oca

Iterative Model and Trajectory Refinement for Orbital Trajectory Optimization

Jennifer S. Hudson[1] * Rohit Gupta[2], Nan Li[2], Ilya V. Kolmanovsky[2]

[1]*Department of Mechanical and Aerospace Engineering, Western Michigan University, Kalamazoo, MI 49009-5343, USA*
[2]*Department of Aerospace Engineering, University of Michigan, Ann Arbor, MI 48109-2140, USA*

SUMMARY

An iterative model and trajectory refinement (IMTR) strategy is proposed for trajectory optimization of nonlinear systems. A high-fidelity model and a low-fidelity model are used. The high-fidelity model accurately represents the system but is not easily amenable to trajectory optimization, due to degree of nonlinearity, computational cost, or to being of "black-box" type. The low-fidelity model is suitable for numerical optimization, but approximates the system dynamics with an error. The IMTR method is proposed to systematically iterate between the two models and efficiently converge on a control solution. Examples are drawn from orbital mechanics. The IMTR approach is compared to optimal nonlinear quadratic control using Pontryagin's maximum principle. A convergence criterion for the IMTR iterations is established.

Received …

KEY WORDS: iterative/numerical methods, optimal control, orbital trajectory optimization

1. INTRODUCTION

It is common in many applications for a system to be described by multiple models of varying fidelity and complexity. Often a high-fidelity model accurately represents the system dynamics but is computationally complex and requires long simulation time. These conditions can make trajectory optimization difficult. Numerical optimization methods require many iterations and, in the absence of a good initial guess, they may not converge.

A low-fidelity model of the system may be more amenable to trajectory optimization. Such a model requires a shorter simulation time and can be optimized by analytical methods (e.g., LQ optimal control, if the low-fidelity model is linear and the cost is quadratic). However, the low-fidelity model does not accurately represent the full system dynamics, and an optimal control derived from the low-fidelity model alone may not achieve the desired system output.

*Correspondence to: Department of Mechanical and Aerospace Engineering, Western Michigan University, Kalamazoo, MI 49009-5343.

Prepared using ocaauth.cls *[Version: 2010/03/27 v2.00]*

Iterative Model and Trajectory Refinement (IMTR) is a recently-proposed trajectory optimization strategy [1, 2] that systematically uses both a high-fidelity and a low-fidelity model of a system. The method uses intertwined steps of trajectory optimization on the low-fidelity model and disturbance estimation to make the low-fidelity model locally match the high-fidelity model. Compared to numerical optimization of the high-fidelity model alone, fewer simulations of the high-fidelity model may be required, which reduces computational costs.

This paper considers the application of IMTR to two spacecraft maneuvering problems in which spacecraft dynamics are represented by both low-fidelity and high-fidelity models: an orbital transfer problem, and a problem of optimal control near libration points in the three-body problem. The orbital transfer problem can be described by nonlinear equations of two-body orbital motion, or the dynamics can be approximated by the linear Clohessy-Wiltshire equations [3]. Spacecraft dynamics near a libration point can be described by the nonlinear circular restricted three-body model, or approximated by linearized equations for perturbation about the equilibrium.

We address the orbital transfer problem using two different approaches. The first uses nonlinear quadratic (NLQ) control with Pontryagin's maximum principle (hereafter, called the maximum principle) to minimize a quadratic cost function of the high-fidelity trajectory. The second approach uses IMTR to optimize the same quadratic cost function through optimization of the low-fidelity model.

Having validated IMTR in comparison with the maximum principle solution in the orbital transfer problem, we address the problem of spacecraft dynamics near a libration point using the IMTR approach only.

In both of our spacecraft examples, the dynamics are highly nonlinear for large maneuvers; the linearization-based low-fidelity model alone is not sufficiently accurate. As we demonstrate, however, such a model can lead to effective, precise, and near-optimal maneuvers once enhanced with IMTR.

A preliminary study of IMTR for spacecraft trajectory optimization has appeared in [4, 5]. The present paper presents a significantly more in-depth treatment of the case studies, and derives theoretical conditions for IMTR iterations convergence.

This paper focuses on high-fidelity models that are nonlinear and low-fidelity models that are linear time-invariant with additive, time-dependent disturbance input. Thus the low-fidelity models are not required to be time-varying linearizations of the system around a nominal trajectory. This approach reduces the trajectory optimization problem to a repeated solution of an LQ-type problem, where a significant portion of the solution can be pre-computed offline.

There is a growing interest in solving the LQ problem for uncertain systems [6]. The proposed approach is related to Iterative Learning Control (ILC) [7, 8] and Iterative Dynamic Programming (IDP) [9]. These techniques are different from IMTR: ILC primarily addresses trajectory tracking where the target trajectory is known rather than an optimal control problem, and neither ILC nor IDP exploit cost minimization based on low-fidelity and high-fidelity dynamic models as considered in IMTR. The proposed approach is also related to iterative schemes for solving optimal control problems for bilinear systems [10, 11, 12, 13], however, IMTR is not limited to high-fidelity models of a particular form.

The paper is organized as follows. In Section 2, the IMTR algorithm is described. Section 3 analyzes IMTR iterations convergence and derives sufficient conditions under which this

Prepared using ocaauth.cls
DOI: 10.1002/oca

convergence takes place. An example for which these sufficient conditions are satisfied is provided. In Section 4, a condition is given under which the solution obtained by IMTR is guaranteed to be a near-optimal solution, i.e., it deviates from the optimal solution of the high-fidelity model by less than a bound. In Section 5, the NLQ and IMTR methods are applied to an example of orbital maneuvering optimal control problem. In Section 6, the IMTR approach is applied to an example of optimal control about the L_4 Lagrange point in the Earth-Moon system. Following the examples, concluding remarks are made in Section 7.

Trajectory optimization is an inherent part of mission planning for spacecraft applications (see, e.g., [14]). While it is a common practice to use different levels of models and approximations in spacecraft trajectory design (e.g., patched conics followed by optimization on a higher fidelity nonlinear simulation model), this is done heuristically and differently from IMTR. In the present paper, we set up an iterative process where the low-fidelity model is tunable and matched to the higher fidelity model in each iteration, and the optimization is performed only on the low-fidelity model.

Spacecraft trajectory optimization is one of many possible areas of application for IMTR. Similar computational strategies can be exploited in other trajectory optimization problems, where the dynamic system can be represented by low-fidelity and high-fidelity models. As an example, in [1] IMTR strategy is applied to clutch trajectory optimization in an automotive vehicle, where the low-fidelity and high-fidelity models are of drastically different orders and complexity. In [2], IMTR is applied to a nonlinear engine control problem with the low-fidelity model based on a linearization at a given operating point.

The numerical examples in this paper and further references [1, 2] indicate that the IMTR strategy can be successful in treating a variety of practical optimal control problems. The analysis in Section 3 establishes sufficient conditions for the IMTR iterations to converge.

2. THE ITERATIVE MODEL AND TRAJECTORY REFINEMENT ALGORITHM

We consider a system described by a nonlinear, high-fidelity, state-space model,

$$\dot{x}_h = f(x_h, u), \tag{1}$$

where x_h is a vector of state variables and u is the manipulated input. The system is also approximated by a linear low-fidelity model,

$$\dot{x}_l = Ax_l + Bu + d, \tag{2}$$

where x_l is a vector of state variables, A and B are constant matrices, and d is a time-dependent disturbance input that we iteratively adjust to improve the match between (1) and (2). The subscripts l and h designate the low-fidelity and high-fidelity models, respectively. While extensions are possible, the dimensionalities of the state and control vectors are assumed to be the same for both the low-fidelity and high-fidelity models. The initial conditions are fixed and $x_h(0) = x_l(0)$.

It is assumed that the high-fidelity model (1) accurately describes the system, while the low-fidelity model (2) describes the system with an error. Note that the linear model is not required

Prepared using ocaauth.cls
DOI: 10.1002/oca

to be a time-varying linearization about the high-fidelity model trajectory. While the low-fidelity model (2) may be defined as a linearization of the nominal model about some nominal (possibly equilibrium) state and control values, it is not required to be.

The objective is to find the control $u(t)$, defined over the time interval $t \in [0, T]$, that minimizes a quadratic cost function,

$$J_h = \frac{1}{2} x_h(T)^T K_f x_h(T) + \frac{1}{2} \int_0^T [x_h(t)^T Q x_h(t) + u(t)^T R u(t)] dt, \tag{3}$$

where $Q^T = Q \geq 0$, $R^T = R > 0$, and $K_f^T = K_f > 0$.

The optimal solution to (3) is not readily available, as the high-fidelity model is nonlinear. However, a similar problem for the linear low-fidelity model (2),

$$J_l = \frac{1}{2} x_l(T)^T K_f x_l(T) + \frac{1}{2} \int_0^T [x_l(t)^T Q x_l(t) + u(t)^T R u(t)] dt, \tag{4}$$

can be solved easily. The optimal solution to the problem of minimizing (4) is given by

$$u = -R^{-1} B^T P x_l + R^{-1} B^T r, \tag{5}$$

where P and r are given by

$$-\dot{P} = A^T P + P A - P B R^{-1} B^T P + Q, \tag{6}$$

$$-\dot{r} = (A - B R^{-1} B^T P)^T r - P d, \tag{7}$$

with $P(T) = K_f$ and $r(T) = 0$ (see, e.g, [15]). Note that (6) is a Riccati equation, the solution of which can be computed independently of the iterative optimization process.

The IMTR algorithm is summarized in Table I. Let the superscript n indicate the iteration number.

Table I. IMTR Algorithm

1.	Initialize the disturbance for the first iteration, d^0.
2.	Solve the finite horizon LQ problem for the low-fidelity model to obtain u^n and x_l^n.
3.	Apply u^n to the high-fidelity model to obtain x_h^n.
4.	Compare x_l^n and x_h^n. Update the disturbance.
5.	Repeat steps 2 through 4 until the algorithm converges.

The disturbance may be initialized at zero or any other reasonable value. During each iteration, IMTR solves the low-fidelity optimization problem and estimates the disturbance $d(t)$. The disturbance update is given by

$$d^{n+1}(t) = d^n(t) + k(\hat{\dot{x}}_h^n(t) - \hat{\dot{x}}_l^n(t)), \tag{8}$$

where $\hat{\dot{x}}_h^n(t)$ is the estimate of the time rate of change of x_h given by the right hand side of (1) with $x_h = x_h^n$, $u = u^n$, and $\hat{\dot{x}}_l^n(t)$ is given by (2) with $u = u^n$, $d = d^n$. The estimate of the time rate of change of x_h^n, $\hat{\dot{x}}_h^n(t)$, can be obtained by evaluating the right hand side of (1) on x_h^n and u^n. The

Prepared using ocaauth.cls
DOI: 10.1002/oca

estimate of the time rate of change of x_l^n, $\hat{\dot{x}}_l^n(t)$, can be obtained by evaluating the right hand side of (2) on x_l^n, u^n, d^n. Alternatively, standard numerical differentiation or filtering techniques can be applied to obtain $\hat{\dot{x}}_h^n(t)$ and $\hat{\dot{x}}_l^n(t)$.

The refinement of $d(t)$ causes the low-fidelity model to match the high-fidelity model more closely with each iteration. The constant k is a gain controlling the change in the disturbance estimate with each iteration. Typically, a value of k between 0 and 1 is chosen.

In principle, (8) may be replaced by updating parameters in a parametric disturbance representation of the form,

$$d(t) = \sum_{i=1}^{m} \theta_i \phi_i(t), \tag{9}$$

where $\phi_i(t)$ are given basis functions and θ_i are estimated parameters.

Each iteration of the IMTR algorithm requires only one simulation of the high-fidelity model. We are never required to numerically optimize the high-fidelity model; all optimization is performed on the low-fidelity model.

Remark 1

Step 3 of the IMTR algorithm can be modified to include a check for decreasing high-fidelity model cost, J_h. After obtaining u^n on the low-fidelity model and applying it to the high-fidelity model, if J_h has increased, the control reverts to u^{n-1}. The disturbance alone is updated until the low-fidelity model reaches a form for which the optimal control also gives a decrease in J_h. This modification ensures that algorithm iterations only give a decrease in the cost and the disturbance estimate is updated multiple times between control updates. The orbital transfer problem in Section 5 uses this approach.

Remark 2

In this paper, the dimensionalities of the states of (1) and (2) are assumed to be the same. A generalization of the IMTR strategy to cases where these dimensions are not the same and when the cost function (3) is non-quadratic can be made. See, for instance, our paper [1] that addresses optimal control of a transmission clutch based on a high order model. The treatment of convergence in such problems could be considerably more involved.

Remark 3

Note that d is a function of time only and not of state; this leads to simple and fast updates, as the low-fidelity model remains linear with time-dependent disturbance input. If d could be chosen as a function of state in (2), a trivial choice $d = f(x_h, u) - Ax_l - Bu$ would provide a perfect match between the low-fidelity and high-fidelity models; however, this choice, clearly, does not address the underlying challenge of solving the optimal control problem.

3. IMTR CONVERGENCE

In this section, we demonstrate that under appropriate assumptions, the iterations of the IMTR algorithm are expected to converge. While this analysis does not demonstrate that the iterations converge to the optimal solution for the high-fidelity model (and in general, examples where this

Prepared using ocaauth.cls
DOI: 10.1002/oca

is not true can be constructed), this convergence is clearly a desirable property as it implies that iterations do not diverge.

At the iteration n, the optimal control for the low-fidelity model is given by

$$u^n = -R^{-1}B^T P x_l^n + R^{-1}B^T r^n, \tag{10}$$

while, with this optimal control, the closed-loop low-fidelity model is given by

$$\dot{x}_l^n = (A - BR^{-1}B^T P)x_l^n + BR^{-1}B^T r^n + d^n. \tag{11}$$

We define the λ_1-norm and λ_2-norm for a function $g(\cdot) \in C^0([0,T])$ as follows

$$\|g\|_{\lambda_1} = \sup_{t\in[0,T]} e^{-\lambda t}\|g(t)\|, \tag{12}$$

$$\|g\|_{\lambda_2} = \sup_{t\in[0,T]} e^{-\lambda(T-t)}\|g(t)\|, \tag{13}$$

where $\lambda > 0$. Note that the sup-norm overbounds and underbounds the λ_1-norm and λ_2-norm for a function $g(\cdot) \in C^0([0,T])$ as follows

$$e^{-\lambda T}\|g\|_\infty \le \|g\|_{\lambda_1} \le \|g\|_\infty,$$
$$e^{-\lambda T}\|g\|_\infty \le \|g\|_{\lambda_2} \le \|g\|_\infty,$$

where the sup-norm is defined as follows

$$\|g\|_\infty = \sup_{t\in[0,T]} \|g(t)\|.$$

While, in principle, it is possible to develop results without introducing the norms (12) and (13), as they are equivalent to the standard sup-norm, the use of the norms (12) and (13) simplifies the application of the contraction mapping-type arguments in the convergence analysis and makes these arguments more elegant. An added advantage of using the norms (12) and (13) is that one can try to adjust the parameter λ in order to satisfy the sufficient conditions for convergence.

The subsequent development of various bounds proceeds under the following assumption.

Assumption 1: Let $f : \mathbb{R}^n \times \mathbb{R}^m \to \mathbb{R}^n$ in (1) be a globally Lipschitz continuous function so that

$$\|f(x,u) - f(y,v)\| \le L_1\|x - y\| + L_2\|u - v\| \tag{14}$$

for all x, $y \in \mathbb{R}^n$ and u, $v \in \mathbb{R}^m$.

The derivation of conditions for IMTR convergence consists of several steps that are now explained at a high level. The reader is referred to Appendix A for details.

DOI: 10.1002/oca

Based on (1), (2) and (8), the bound on the change in the disturbance between two consecutive iterations is given by

$$\|d^{n+1} - d^n\|_{\lambda_1} \leq m_1\|d^n - d^{n-1}\|_{\lambda_1} + m_2||r^n - r^{n-1}||_{\lambda_2} + m_3\|x_l^n - x_l^{n-1}\|_{\lambda_1} + m_4\|x_h^n - x_h^{n-1}\|_{\lambda_1}, \tag{15}$$

where $m_1 > 0$, $m_2 > 0$, $m_3 > 0$, and $m_4 > 0$ are appropriately defined. Then based on (7), it can be shown that there exists $m_5 > 0$ such that

$$\|r^{n+1} - r^n\|_{\lambda_2} \leq m_5\|d^{n+1} - d^n\|_{\lambda_1}. \tag{16}$$

In turn, based on (11), it can be shown that there exists $m_6 > 0$ and $m_7 > 0$ such that

$$\|x_l^{n+1} - x_l^n\|_{\lambda_1} \leq m_6\|d^{n+1} - d^n\|_{\lambda_1} + m_7\|r^{n+1} - r^n\|_{\lambda_2}. \tag{17}$$

It follows from (1), (5) that

$$\|x_h^{n+1} - x_h^n\|_{\lambda_1} \leq m_8\|r^{n+1} - r^n\|_{\lambda_2} + m_9\|x_l^{n+1} - x_l^n\|_{\lambda_1}. \tag{18}$$

From the inequalities (15)-(18), it follows that there exists $\alpha > 0$ such that

$$\|d^{n+1} - d^n\|_{\lambda_1} \leq \alpha\|d^n - d^{n-1}\|_{\lambda_1}. \tag{19}$$

The value of α is given by (44) in Appendix A. The following result can now be stated.

Proposition 1

Suppose $\alpha \in (0, 1)$, where α is given by (44). Then the iterations of the IMTR algorithm converge. Specifically, $\lim_{n\to\infty} d^n = d^\infty$, $\lim_{n\to\infty} r^n = r^\infty$, $\lim_{n\to\infty} x_l^n = x_l^\infty$ and $\lim_{n\to\infty} x_h^n = x_h^\infty$ uniformly on $[0, T]$ for appropriate continuous functions, d^∞, r^∞, x_l^∞ and x_h^∞, respectively. Moreover, $\lim_{n\to\infty} \|x_h^n - x_l^n\|_\infty = 0$, $J_l^\infty = \lim_{n\to\infty} J(x_l^n) = \lim_{n\to\infty} J(x_h^n) = J_h^\infty$.

Proof

See Appendix B. □

Remark 4

The condition in Proposition 1 is sufficient and requires the computation of α. We generally expect that small values of k are conducive to being able to satisfy this condition and achieve IMTR convergence. For the example in Section 5.3, we provide a numerical study of the dependence of α on k, and we leave further study of this dependence to future work.

Remark 5

Proceeding a bit further, it is also possible to obtain a characterization of the low-fidelity model cost change over one iteration, $J_l^{n+1} - J_l^n$ as a quadratic function of $k > 0$ in (8). Specifically, the update equations can be written as follows,

$$d^{n+1}(t) = d^n(t) + k\dot{e}^n(t),$$
$$r^{n+1}(t) = r^n(t) + k\phi^n(t),$$

Prepared using ocaauth.cls
DOI: 10.1002/oca

with $\phi^n(t)$ satisfying the following differential equation,

$$-\dot{\phi}^n = \tilde{A}^T\phi^n - \tilde{B}\dot{e}^n, \quad \phi^n(T) = 0,$$

where $\dot{e}^n = \dot{x}_h^n - \dot{x}_l^n$ and $\tilde{A}$, $\tilde{B}$ are defined in Appendix A. Based on (4)-(7), it can be shown (see, e.g., [16, p. 76])

$$J_l^{n+1} - J_l^n = -k^2 \int_0^T [\phi^{nT}(\tau)\dot{e}^n(\tau) + \frac{1}{2}\phi^{nT}(\tau)BR^{-1}B^T\phi^n(\tau)]d\tau$$
$$- k\left[\phi^{nT}(0)x_l^n(0) + \int_0^T [r^{nT}(\tau)\dot{e}^n(\tau) + \phi^{nT}(\tau)d^n(\tau) + \phi^{nT}(\tau)BR^{-1}B^T r^n(\tau)]d\tau\right].$$

The ability to easily predict the change in the low-fidelity model cost as a function of k may be exploited in strategies for online selection of k. We leave the development of such strategies to future work, while our subsequent examples use a constant k.

Remark 6
IMTR is a computational strategy and convergence may not be expected for all types of problems. Computational studies and further numerical analysis need to be undertaken to understand whether highly divergent, in particular, chaotic systems may be amenable to this strategy.

3.1. Example

We now provide an example to demonstrate the sufficient condition in Proposition 1. In this example, the high-fidelity model is a scalar nonlinear system, while the corresponding low-fidelity model is the linearization of the high-fidelity model at the origin plus a disturbance. Specifically, the high-fidelity model and the corresponding low-fidelity model are given as

$$\dot{x}_h = -0.1\sin x_h + 0.05u,$$
$$\dot{x}_l = -0.1x_l + 0.05u + d.$$

The cost function is given by (3) with $Q = 1$, $R = 1$ and $K_f = 10$. One set of parameters that satisfies the sufficient condition in Proposition 1 is given by

$$\lambda = 0.6,$$
$$k = 0.1,$$
$$T = 2,$$

which yields

$$\alpha = 0.9635 \in (0, 1). \tag{20}$$

The reader is referred to Appendix C for details. Thus, the sufficient condition in Proposition 1 holds and we also confirm the convergence by numerical simulations. Fig. 1 shows the evolution of trajectories during the iterations of IMTR. The blue and red trajectories correspond to the low-fidelity and high-fidelity models, respectively, while the final trajectory after 100 iterations is shown in green.

Prepared using ocaauth.cls
DOI: 10.1002/oca

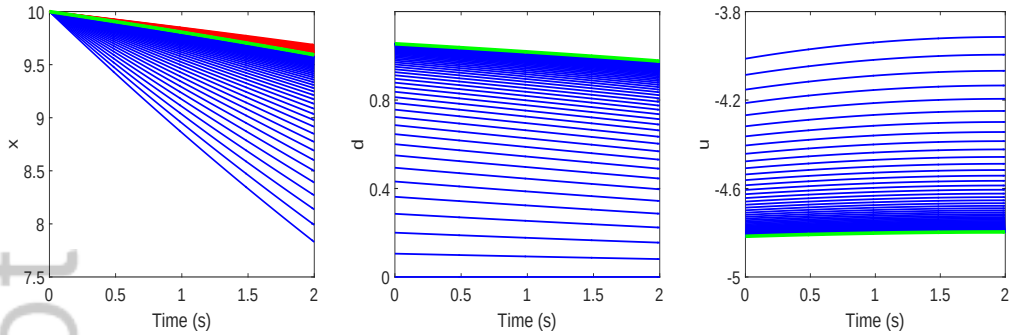

Figure 1. An example to demonstrate the sufficient condition in Proposition 1. Left: High and low-fidelity model trajectories. Middle: Disturbance trajectories. Right: Control trajectories.

4. NEAR-OPTIMAL SOLUTION BY IMTR

The control trajectory obtained by IMTR may be different from the optimal control for the high-fidelity model, obtained, e.g., by the maximum principle and the solution of the resulting two-point boundary value problem. By the algorithm modification in Remark 1, a cost decrease for the high-fidelity model is guaranteed after each control update. In several examples, we have noticed that the solution of IMTR is close to the solution of the original optimal control problem. Motivated by this observation, we provide the following conditions supporting the expectation for the near-optimality of IMTR solution under certain assumptions.

Proposition 2
Suppose the nonlinear high-fidelity model is of the following form,

$$\dot{x}_h = Ax_h + Bu + d_h(x_h, t), \tag{21}$$

where A and B are the same as in (2), and that there exists $\bar{d}(t)$ such that

$$\|d_h(x_h, t) - \bar{d}(t)\| \leq \epsilon, \tag{22}$$

for some $\epsilon > 0$ and for all values of x_h. Then assuming IMTR iterations converge in the sense of Proposition 1, the deviation of the optimal cost (3) from the cost (3) evaluated on the trajectories obtained by IMTR is $O(\epsilon)$ for ϵ sufficiently small.

Proof
See Appendix D. □

Remark 7
It is clear from the proof of Proposition 2 that (22) needs to only hold for the values of x_h in the set which bounds the optimal trajectory of the high-fidelity model and the trajectory to which IMTR converges. While we leave further investigation of conditions under which near-optimality of IMTR solutions can be assured to future research, in the next sections, we investigate two case studies to numerically show that near-optimal solutions can be obtained through IMTR techniques.

Prepared using ocaauth.cls
DOI: 10.1002/oca

5. ORBITAL TRANSFER

The problem of optimal control of a low-thrust spacecraft orbital transfer maneuver is used to compare the NLQ and IMTR approaches. A target orbit is a circular Earth orbit with radius R_0 and constant orbital angular velocity $\dot{\theta} = \sqrt{\frac{\mu}{R_0^3}}$. A spacecraft in a different initial orbit must be controlled to match the orbital radius and velocity of the target orbit at a fixed final time.

The high-fidelity model is the classical two-body model, with the equations of motion written in polar coordinates as [17]:

$$\ddot{r} - r\dot{\theta}^2 = -\frac{\mu}{r^2} + a_r, \tag{23}$$

$$r\ddot{\theta} + 2\dot{r}\dot{\theta} = a_\theta, \tag{24}$$

where r is the distance from the center of the Earth to the spacecraft, θ is the polar angle, and a_r and a_θ are the thrust accelerations in the radial ($\hat{r}$) and tangential ($\hat{\theta}$) directions, respectively.

The system state is

$$x = \begin{bmatrix} x_1 \\ x_2 \\ x_3 \\ x_4 \end{bmatrix}, \tag{25}$$

where $x_1 = r$, $x_2 = \dot{r}$, $x_3 = \theta$, $x_4 = \dot{\theta}$. The control is defined by the acceleration components,

$$u = \begin{bmatrix} a_r \\ a_\theta \end{bmatrix}. \tag{26}$$

The low-fidelity model uses the linearized two-body orbital equations of motion, known as the Clohessy-Wiltshire equations [3] in the form given in [17]:

$$\Delta\ddot{r} = 3n^2\Delta r + 2nR_0\Delta\dot{\theta} + a_r, \tag{27}$$

$$R_0\Delta\ddot{\theta} = -2n\Delta\dot{r} + a_\theta. \tag{28}$$

This is a linear model with state variables Δr and $\Delta\theta$ representing perturbations of the spacecraft radial distance and polar angle from an (imagined) spacecraft on the target circular orbit. The state trajectory of the (imagined) spacecraft on the target circular orbit is denoted by $\dot{x}_{target}$.

5.1. Maximum Principle Solution

The optimal orbital transfer control problem is first solved using NLQ control. A finite horizon cost is defined

$$J = \frac{1}{2}(x(T) - x_T)^T K_f (x(T) - x_T) + \frac{1}{2}\int_0^T [(x(\tau) - x_T)^T Q(x(\tau) - x_T) + u(\tau)^T R u(\tau)]d\tau, \tag{29}$$

Prepared using ocaauth.cls
DOI: 10.1002/oca

where T is the final time and x_T is the target state. To minimize the cost, the maximum principle is used. The Hamiltonian for the minimization problem is

$$H = \frac{1}{2}(x - x_T)^T Q(x - x_T) + \frac{1}{2}u^T Ru + p_1 x_2 + p_2 \left(x_1 x_4^2 - \frac{\mu}{x_1^2} + a_r \right) + p_3 x_4 + p_4 \frac{1}{x_1}(-2x_2 x_4 + a_\theta),$$

where p_1, p_2, p_3, and p_4 are the adjoint variables. The first-order necessary conditions for optimality are

$$\frac{\partial H}{\partial u} = Ru + \begin{bmatrix} p_2 \\ \frac{p_4}{x_1} \end{bmatrix} = 0.$$

Therefore, the optimal control is given by

$$u = -R^{-1} \begin{bmatrix} p_2 \\ \frac{p_4}{x_1} \end{bmatrix}.$$

The adjoint equations are

$$\dot{p} = -\left(\frac{\partial H}{\partial x} \right)^T = -Q(x - x_T) - \begin{bmatrix} p_2 x_4^2 + 2\frac{p_2 \mu}{x_1^3} - \frac{p_4}{x_1^2}(-2x_2 x_4 + a_\theta) \\ p_1 - 2\frac{p_4}{x_1} x_4 \\ 0 \\ 2p_2 x_1 x_4 + p_3 - 2\frac{x_2}{x_1} p_4 \end{bmatrix}.$$

The transversality conditions are

$$p(T) = K_f(x(T) - x_T). \tag{30}$$

The two-point boundary value problem is solved for $x(0)$ and $p(0)$ such that (30) holds.

5.2. IMTR Solution

The IMTR control solution to the orbital transfer problem is found using the approach described in Section 2. The high-fidelity model is given by (23) and (24) with a state vector x_h given by (25). The low-fidelity model is given by (27) and (28). The low-fidelity state is given by perturbations of the spacecraft from the target,

$$x_l = \begin{bmatrix} \Delta r \\ \Delta \dot{r} \\ \Delta \theta \\ \Delta \dot{\theta} \end{bmatrix}.$$

Consistently with the low-fidelity model based on the Clohessy-Wiltshire equations (27) and (28), the disturbance to be added to the low-fidelity model is based on the difference in the dynamics of

Prepared using ocaauth.cls
DOI: 10.1002/oca

the perturbed state,

$$d^{n+1}(t) = d^n(t) + k[(\hat{\dot{x}}_h^n(t) - \dot{x}_{target}(t)) - \hat{\dot{x}}_l^n(t)],$$

where $x_{target}(t)$ represents the state trajectory of an (imagined) spacecraft on the target circular orbit.

The low-fidelity and high-fidelity model costs are calculated using (29) with x given by $(x_h - x_{target})$ and x_l, respectively. The IMTR algorithm is applied with the modification described in Remark 1 of Section 2, i.e., only the disturbance – not the control – is updated during iterations in which the control update would increase the high-fidelity model cost.

5.3. Orbital Transfer Example

Figures 2 - 6 show an example of the maximum principle and IMTR applied to the targeting problem with

$$x_0 = \begin{bmatrix} R_e + 1400 \\ 0 \\ 0 \\ \sqrt{\dfrac{\mu}{(R_e+1400)^3}} \end{bmatrix},$$

$$x_T = \begin{bmatrix} R_e + 2000 \\ 0 \\ 0 \\ \sqrt{\dfrac{\mu}{(R_e+2000)^3}} \end{bmatrix},$$

i.e., a spacecraft transferring from a 1,400 km circular orbit to a 2,000 km circular orbit. Note that a 600 km orbit transfer maneuver is large and the Clohessy-Wiltshire equations alone are not accurate at such distances to plan an accurate maneuver. As we will demonstrate, accurate maneuvers can be achieved using IMTR.

The transfer time T is the orbit period of the target, $T = 7,631$ seconds $= 2.12$ hours. The penalty on the final state is

$$K_f = \begin{bmatrix} 1 & 0 & 0 & 0 \\ 0 & 1 & 0 & 0 \\ 0 & 0 & 0 & 0 \\ 0 & 0 & 0 & 1 \end{bmatrix},$$

which avoids penalizing the polar angle $x_3 = \theta$. This represents an orbit-raising problem, with no constraint on the final angular position of the spacecraft. In this example, Q is set to zero, because non-zero Q makes the adjoint equations stiff and R is

$$R = \begin{bmatrix} 10^9 & 0 \\ 0 & 10^9 \end{bmatrix},$$

Prepared using ocaauth.cls
DOI: 10.1002/oca

which was found to yield solutions with low thrust accelerations (existing electric propulsion systems typically produce less than 1 N of thrust [18, 19], while developmental systems may be able to produce up to 15 N [20]). The parameter value $k = 0.2$ was selected to limit the change in d from one iteration to the next.

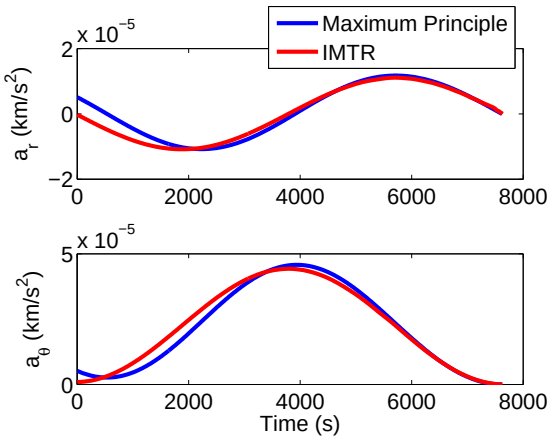

Figure 2. Commanded acceleration in orbital transfer problem.

Figure 2 shows the optimal control inputs a_r and a_θ calculated by both the maximum principle and the IMTR strategy. The results are similar, but not identical.

Figure 3 shows the cost (29) calculated by the low-fidelity and high-fidelity models during each iteration of the IMTR algorithm, compared to the optimal cost calculated by the maximum principle. The low-fidelity model cost varies as the disturbance updates improve the low-fidelity model match over several iterations. The high-fidelity model cost decreases in several steps.

In this example, the IMTR algorithm termination criterion was that J_h change by less than 1% of its final value over the previous two decreasing steps. This criterion was satisfied after 164 iterations. This number of iterations is reasonable compared to other iterative trajectory optimization methods.

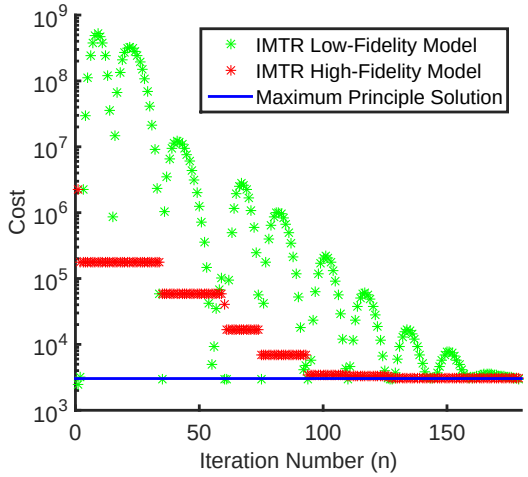

Figure 3. Cost in orbital transfer problem.

DOI: 10.1002/oca

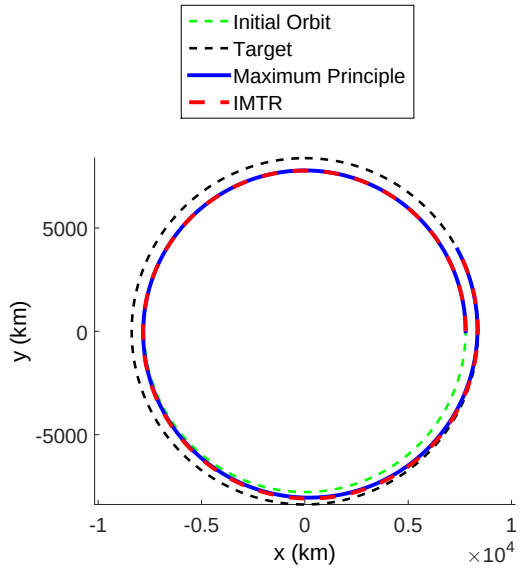

Figure 4. Planar (x, y) trajectories in orbital transfer problem.

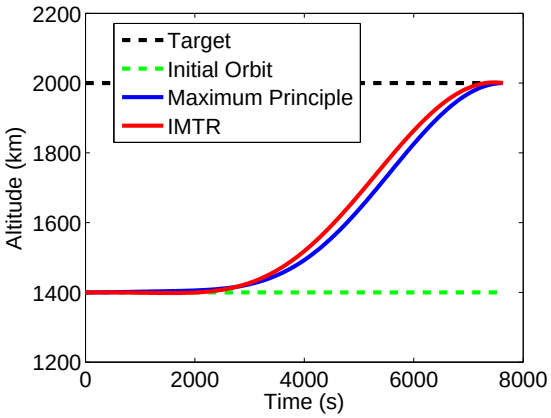

Figure 5. Altitude in orbital transfer problem.

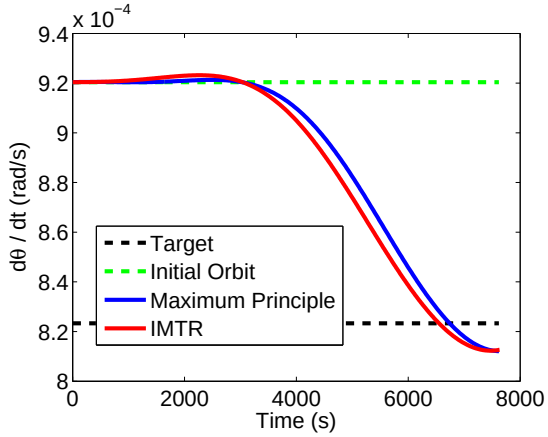

Figure 6. Angular rate in orbital transfer problem.

Prepared using ocaauth.cls
DOI: 10.1002/oca

For example, Reference [21] used an SQP algorithm to solve a low-thrust orbital trajectory problem with two formulations requiring 125 and 263,340 iterations, respectively.

The control solution from the maximum principle approach had a maximum total acceleration of 0.0458 m/s^2, where total acceleration is

$$a_{total}(t) = \sqrt{a_r(t)^2 + a_\theta(t)^2}.$$

This maximum acceleration corresponds to a thrust of 13.7 N for a 300 kg spacecraft. The control solution from the IMTR approach had a maximum total acceleration of 0.0443 m/s^2. This maximum acceleration corresponds to a thrust of 13.3 N for a 300 kg spacecraft. Both methods achieved approximately the same optimal cost; $J = 3,033$ for the maximum principle solution and $J = 3,072$ for the IMTR solution.

Figure 4 shows the orbital trajectories resulting from the maximum principle and the IMTR solution. The two solutions overlap closely.

Figures 5 and 6 show the resultant time-histories of orbit altitude and angular rate from the maximum principle and IMTR. The results are very similar for both methods; the maximum principle yields a slightly slower solution, but the final states are very similar. Both methods reach the target radius but miss the target angular rate by about $1 \cdot 10^{-5}$ rad/s. This is the result of our choice of Q, R, and K_f; a small miss in $\dot{\theta}$ achieved the lowest total cost. A more accurate solution, at the expense of a higher control cost, could be obtained by adjusting these matrices.

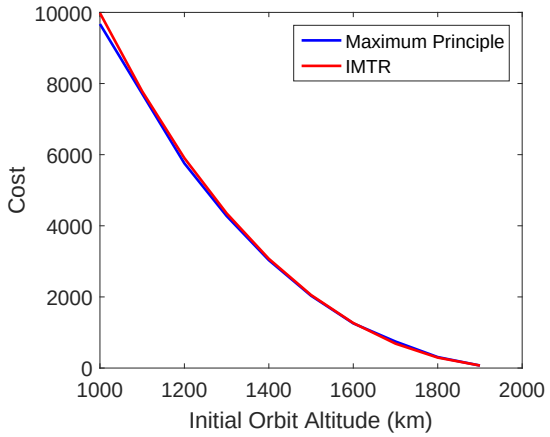

Figure 7. Cost vs. initial altitude in orbital transfer problem.

Figures 7 and 8 show the results of the maximum principle and the IMTR strategy for a range of initial conditions. The orbital transfer problem with a target altitude of 2,000 km was solved for initial altitudes ranging from 1,000 km to 1,900 km. In the IMTR solutions, the parameter value $k = 0.5$ was used. All other problem parameters were maintained at the values given above. Each problem was terminated when J_h changed by less than 1% over two sequential steps. As expected, the cost and the maximum acceleration decreases for initial conditions closer to the target orbit. The maximum principle and IMTR solutions are very similar; the maximum principle results in slightly lower cost and slightly higher maximum acceleration for the cases with the lowest initial altitude.

DOI: 10.1002/oca

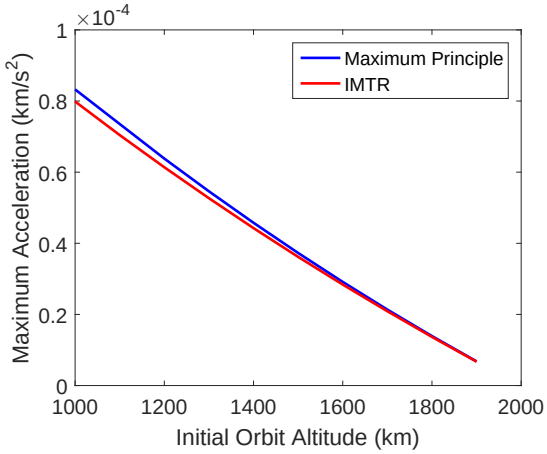

Figure 8. Maximum acceleration vs. initial altitude in orbital transfer problem.

As per Proposition 1, the value of α in (19) determines convergence of the IMTR algorithm. In the orbital transfer example in Figures 2-6, α varies as a function of iteration number n and parameter k. Figure 9 shows the value of α, calculated numerically using (12) with $\lambda = 2$ for this example. For $k \leq 0.1$, we find $\alpha \in (0, 1)$ on every iteration . For $k = 0.2, 0.3, 0.5$, the value of α is generally in this range, but there are exceptions on a few isolated iterations. In these cases, the process returns to $\alpha < 1$ on the next iteration; these exceptions do not prevent convergence. The IMTR algorithm converged for all values of k shown in Figure 9, with a faster rate of convergence for larger values of k.

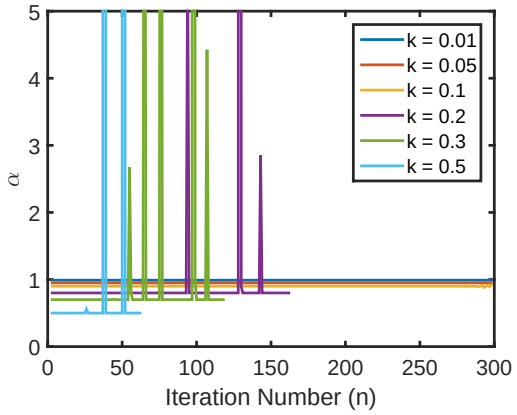

Figure 9. α vs. iteration number in orbital transfer problem.

6. EARTH-MOON L_4 TARGETING

As a second example, we apply the IMTR strategy to the problem of optimally controlling a spacecraft near the L_4 Lagrange point of the Earth-Moon system [17]. The five Lagrange points are the locations in a three-body orbital system where a small body can maintain a constant position

Prepared using ocaauth.cls
DOI: 10.1002/oca

with respect to two larger bodies, as gravitational and centripetal forces cancel. A spacecraft can orbit a Lagrange point and remain in constant alignment with the primary bodies, which makes the Lagrange points useful locations for many space missions.

The nonlinear equations of the planar circular restricted three-body model [17] are the high-fidelity model of the system,

$$\ddot{x} - 2\omega_0\dot{y} - \omega_0^2 x = \frac{\mu_1(x - D_1)}{r_1^3} - \frac{-\mu_2(x + D_2)}{r_2^3} + \eta_x + a_x,$$
$$\ddot{y} + 2\omega_0\dot{x} - \omega_0^2 y = \frac{\mu_1 y}{r_1^3} - \frac{-\mu_2 y}{r_2^3} + \eta_y + a_y,$$

where the coordinate frame is rotating with constant velocity ω_0 about the center of mass of the Earth-Moon system, D_1 is the distance to the Earth from the center along the positive x axis, D_2 is the distance to the Moon from the center along the negative x axis, and μ_1 and μ_2 are the constant gravity parameters of the Earth and Moon, respectively. The perturbations η_x and η_y are added to represent unknown system behavior, such as control disturbances, solar radiation pressure perturbations, and gravitational perturbations. The accelerations a_x and a_y are the control inputs.

The linearized restricted 3-body orbital dynamics for perturbations from L_4 equilibrium [17] are the low-fidelity model of the system,

$$\Delta\ddot{x} = 2\omega_0\Delta\dot{y} + \frac{3}{4}\omega_0^2\Delta x + \frac{3\sqrt{3}}{2}(\rho - \frac{1}{2})\omega_0^2\Delta y + a_x,$$
$$\Delta\ddot{y} = -2\omega_0\Delta\dot{x} + \frac{3\sqrt{3}}{2}(\rho - \frac{1}{2})\omega_0^2\Delta x + \frac{9}{4}\omega_0^2\Delta y + a_y,$$

where Δx and Δy are the components of the position vector of the spacecraft relative to the Lagrange point and ρ is the mass ratio of the Earth-Moon system,

$$\rho = \frac{M_{Moon}}{M_{Earth} + M_{Moon}}.$$

Comparing the two models, the high-fidelity model alone is more difficult and computationally expensive to optimize due to its nonlinear structure. The low-fidelity model is amenable to LQ optimal control, but the solution becomes less accurate as the state moves away from L_4. In the simulations below, the IMTR strategy converges on a solution to the high-fidelity problem from initial points more than 14,000 km away from L_4.

The following examples show an optimal control problem in which the objective is to control the spacecraft from a perturbed initial state to the L_4 point. The initial state perturbation from L_4 is

$$x_l(0) = \begin{bmatrix} \Delta x \\ \Delta y \\ \Delta\dot{x} \\ \Delta\dot{y} \end{bmatrix}.$$

Prepared using ocaauth.cls
DOI: 10.1002/oca

A cost function of the form (29) is defined using the high-fidelity state,

$$x_h = \begin{bmatrix} x \\ y \\ \dot{x} \\ \dot{y} \end{bmatrix}.$$

The final time is fixed at 24 hours. The acceleration perturbations are $\eta_x = 1 \cdot 10^{-9}$ km/s^2 and $\eta_y = 2 \cdot 10^{-9}$ km/s^2. The cost to be minimized is given by (3) with $K_f = I_4$, $Q = I_4$, and

$$R = \begin{bmatrix} 10^{14} & 0 \\ 0 & 10^{14} \end{bmatrix},$$

which was found to yield low thrust acceleration solutions. As in the previous example, the parameter value $k = 0.1$ was selected.

Figures 10-12 show the IMTR strategy applied to the targeting problem with initial conditions $x(0) = 5,000$ km, $y(0) = 5,000$ km, in the rotating frame, relative to L_4. The IMTR algorithm was terminated when the cost (3) varied by less than 10% over three iterations and the final cost was less than any previously calculated cost. This occurred after 55 iterations.

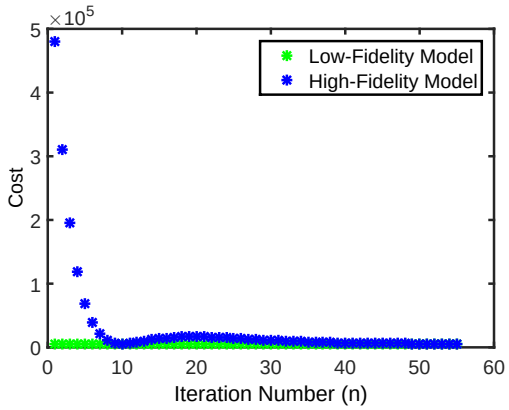

Figure 10. Cost in Earth-Moon L_4 targeting problem.

Figure 10 shows the costs calculated by the low-fidelity and high-fidelity models on each iteration of the IMTR algorithm. The cost decreases sharply over the first ten iterations and then approaches the minimum more slowly over the next 45 iterations.

Figure 11 shows the calculated trajectories at various iterations of the IMTR algorithm. The (x, y) reference frame rotates with the Earth-Moon system. The first trajectory ends far from the target point, which indicates that the low-fidelity model does not solve the problem with this initial condition far from the L_4 point. However, accuracy improves over the iterations and the final trajectory approaches the target.

Figure 12 shows the solution to the problem, the commanded thrust acceleration. The accelerations in the x and y directions are nearly identical.

Figures 13-14 show the results of the same approach for a range of initial conditions. The values of $\Delta x(0)$ and $\Delta y(0)$ varied from -10,050 to 10,050 while $\Delta \dot{x}(0)$ and $\Delta \dot{y}(0)$ were held at zero. The

Prepared using ocaauth.cls
DOI: 10.1002/oca

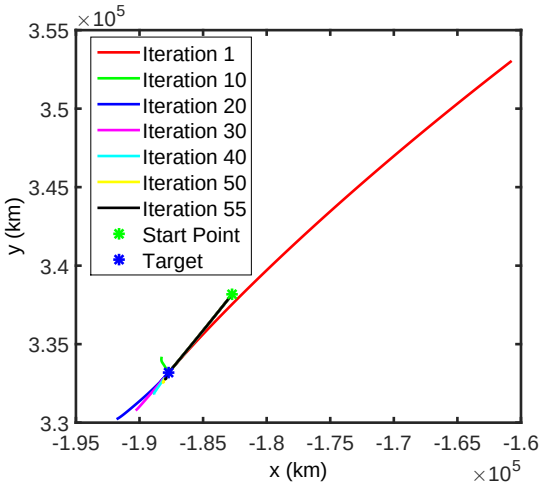

Figure 11. Trajectories in the rotating frame calculated during selected iterations of the IMTR algorithm in Earth-Moon L_4 targeting problem.

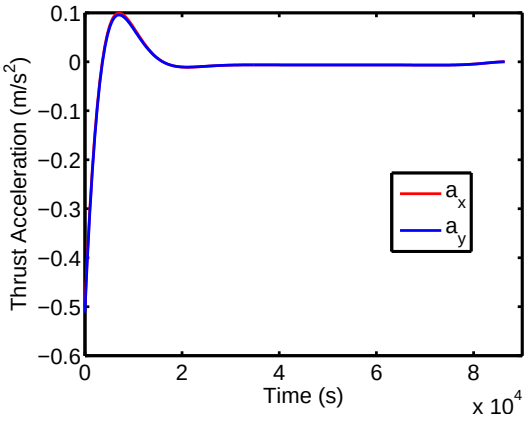

Figure 12. Control solution: thrust acceleration in Earth-Moon L_4 targeting problem.

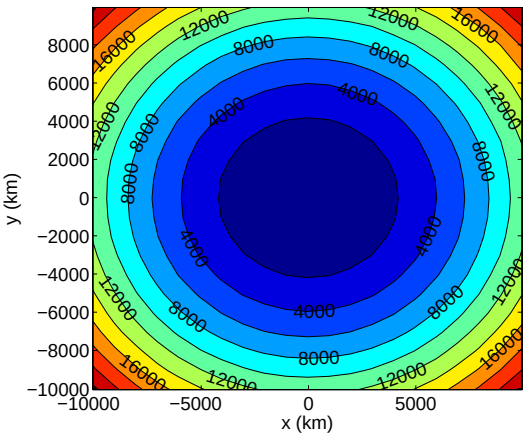

Figure 13. Calculated cost vs. initial position relative to L_4 in Earth-Moon L_4 targeting problem.

DOI: 10.1002/oca

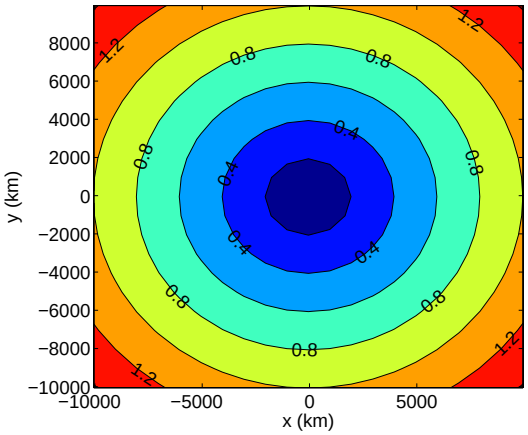

Figure 14. Maximum acceleration (m/s^2) vs. initial position relative to L_4 in Earth-Moon L_4 targeting problem.

final time and the constants η_x, η_y, K_f, Q, and R have the values given above. At each point in the range of $\Delta x(0)$ and $\Delta y(0)$, the spacecraft was initialized with zero velocity relative to the rotating reference frame. The IMTR method was used to calculate the optimal trajectory to the L_4 point. The algorithm converged for each case, with initial distances ranging from 50 km to 14,213 km from L_4.

Figure 13 shows the minimum cost J calculated by the IMTR approach for each initial position relative to the L_4 point. As expected, the cost increases with distance from L_4.

Figure 14 shows the maximum total acceleration required for the trajectory from each initial position, where total acceleration is

$$a_{total}(t) = \sqrt{a_x(t)^2 + a_y(t)^2}.$$

The maximum acceleration ranges from 1.4 m/s^2 at the farthest initial conditions to 0.0105 m/s^2 at the nearest initial conditions. For a 300 kg spacecraft, these maximum accelerations correspond to maximum thrusts of 420 N and 3.15 N, respectively.

7. CONCLUSIONS

This paper presented an IMTR approach to spacecraft trajectory optimization using iterations of low-fidelity and high-fidelity models. Sufficient conditions for IMTR convergence were established. An example of low-thrust spacecraft orbital transfer was described and the IMTR solution was compared to NLQ control based on the maximum principle. A second example of spacecraft control in the three-body Earth-Moon system near the L_4 Lagrange point was also described and solved using the IMTR strategy.

Both examples exercised IMTR for a range of initial conditions and in all cases we have been able to obtain reasonable solutions. In the first example, IMTR calculated a solution very similar to the optimal solution based on the maximum principle. In the second example, IMTR found control solutions for initial conditions far from the point about which the low-fidelity equations were

DOI: 10.1002/oca

linearized. These examples indicate that IMTR can be a useful strategy for many types of trajectory optimization problems with complex, nonlinear dynamics and low-fidelity model representations. In particular, IMTR can be used to warm start Newton-type two point boundary value solvers that are based on necessary conditions for optimality; such solvers require a good initial guess to achieve convergence.

While our examples illustrate the potential for IMTR application to practical trajectory optimization problems, much room remains for further research on conditions under which convergence of IMTR takes place.

ACKNOWLEDGMENTS

Ilya Kolmanovsky and Nan Li acknowledge support of the National Science Foundation Award CNS 1544844.

REFERENCES

1. Hudson, J., Kolmanovsky, I.V., Hong J., Dai, E., McCallum J., Pietron, G., Shelton, M., Iterative model and trajectory refinement for launch optimization of automotive powertrains, *Proceedings of 15th IFAC Workshop on Control Applications of Optimization*, Rimini, Italy, September, 2012.
2. Gupta, R., Hudson, J., Bloch, A.M., and Kolmanovsky, I.V. Optimal control of manifold filling during VDE mode transitions, *Proceedings of the 52nd IEEE Conference on Decision and Control*, Florence, Italy, 2013.
3. Clohessy, W.H., Wiltshire, R.S. Terminal guidance system for satellite rendezvous, *Journal of the Aerospace Sciences* 1960; **27**(9): 653-658.
4. Hudson, J., Kolmanovsky, I., Iterative model refinement for orbital trajectory optimization," *Proceedings of 2012 AAS/AIAA Space Flight Mechanics Meeting*, Charleston, SC, 2012.
5. Hudson, J., and Kolmanovsky, I.V., Iterative model and trajectory refinement for attitude and shape control of a dumbbell spacecraft, *Proceedings of 2013 AAS/AIAA Astrodynamics Specialist Conference*, August 11-15, 2013, Hilton Head, South Carolina, Paper AAS 13-890.
6. Frihauf, P., Krstic, M., Basar, T. Finite-horizon LQ control for unknown discrete-time linear systems via extremum seeking, *Proceedings of 51st IEEE Conference on Decision and Control (CDC)*, Maui, HI, 10-13 Dec. 2012; 5717-5722. doi: 10.1109/CDC.2012.6426052
7. Gunnarsson, S., Norrlof, M. On the design of ILC algorithms using optimization, *Automatica* 2001; **37**(12): 2011-2016. ISSN 0005-1098, 10.1016/S0005-1098(01)00154-6
8. Lee, J.H., Lee, K.S., Kim, W.C. Model-based iterative learning control with a quadratic criterion for time-varying linear systems, *Automatica* 2000, **36**(5): 641-657. ISSN 0005-1098, 10.1016/S0005-1098(99)00194-6
9. Luus, R. On the application of iterative dynamic programming to singular optimal control problems, *IEEE Transactions on Automatic Control* 1992; **37**(11): 1802-1806. doi: 10.1109/9.173155
10. Hofer, E.P., Tibken, B. An iterative method for the finite-time bilinear-quadratic control problem, *Journal of Optimization Theory and Applications* 1998; **57**(3): 411-427. doi:10.1007/BF02346161
11. Ying, Y.Q., Rao, M, and Sun, Y.X. Suboptimal control for bilinear systems, *Optimal Control Applications and Methods* 1993; **14**(3): 195-201. DOI: 10.1002/oca.4660140305
12. Aganovic, Z., Gajic, Z. The successive approximation procedure for finite-time optimal control of bilinear systems. *IEEE Transactions on Automatic Control* 1994; **39**(9): 1932-1935. doi: 10.1109/9.317128
13. Lee, S., Lee, K. Bilinear systems controller design with approximation techniques. *Journal of the Chungcheong Mathematical Society* 2005; **18**(1).
14. Conway, B.A., Spacecraft Trajectory Optimization. Cambridge University Press: Cambridge, 2010.
15. Isidori, A. and Astolfi, A. Disturbance attenuation and H∞ control via measurement feedback in nonlinear systems, *IEEE Transactions of Automatic Control* 1992; **37**(9): 1283-1293.
16. Boltyanski, V.G., Poznyak, A.S. The Robust Maximum Principle: Theory and Applications. Birkhäuser Mathematics: New York, 2012.

Prepared using ocaauth.cls
DOI: 10.1002/oca

17. Wie, B. Space Vehicle Dynamics and Control. AIAA: Reston, VA, 1998.
18. Polk, J. E., Brinza, D., Kakuda, R. Y., Brophy, J. R., Katz, I., Anderson, J. R., Rawlin, V. K., Patterson, M. J., Sovey, J., Hamley, J. Demonstration of the NSTAR ion propulsion system on the Deep Space One mission. *Proceedings of the 27th International Electric Propulsion Conference*, Pasadena, CA, Oct. 2001; also Paper 01-075.
19. Patterson, M. J., Benson, S. W. NEXT ion propulsion system development status and performance. *Proceedings of the 43rd Joint Propulsion Conference and Exhibit*, Cincinnati, OH, 2007; also Paper 2007-5199.
20. Florenz, R. E., Hall, S. J., Gallimore, A. D., Kamhawi, H., Griffiths, C. M., Brown, D. L., Hofer, R. R., and Polk, J. E. First firing of a 100-kW nested-channel hall thruster. *Proceedings of the 33rd International Electric Propulsion Conference*, Washington, DC, 2013. IEPC-2013-394.
21. Betts, J. T. Very low-thrust trajectory optimization using a direct SQP method. *Journal of Computational and Applied Mathematics* 2000; **120**: 27-40.

APPENDIX A: DERIVATION OF (19)

We begin with the following facts.

Fact 1: For all $t \in [0, T]$, the following inequalities hold

$$\begin{aligned}\int_0^t \|g(\tau)\|d\tau &= \int_0^t e^{-\lambda\tau}e^{\lambda\tau}\|g(\tau)\|d\tau \\ &\leq \|g\|_{\lambda_1}\int_0^t e^{\lambda\tau}d\tau, \\ \int_t^T \|g(\tau)\|d\tau &= \int_t^T e^{-\lambda(T-\tau)}e^{\lambda(T-\tau)}\|g(\tau)\|d\tau \\ &\leq \|g\|_{\lambda_2}\int_t^T e^{\lambda(T-\tau)}d\tau.\end{aligned}$$

Fact 2: For all $t \in [0, T]$, the following inequalities hold

$$\begin{aligned}e^{-\lambda t}\int_0^t e^{\lambda\tau}d\tau &\leq \frac{1}{\lambda}, \\ e^{-\lambda(T-t)}\int_t^T e^{\lambda(T-\tau)}d\tau &\leq \frac{1}{\lambda}.\end{aligned}$$

Define the following quantities,

$$c_1 = \sup_{t\in[0,T]}\|\tilde{A}(t)\|, \tag{31}$$

$$c_2 = \sup_{t\in[0,T]}\|\tilde{A}^T(t)\|, \tag{32}$$

$$c_3 = \sup_{t\in[0,T]}\|\tilde{B}(t)\|, \tag{33}$$

$$c_4 = \sup_{t\in[0,T]}\|K_1(t)\|, \tag{34}$$

$$c_5 = \|K_2\|, \tag{35}$$

$$c_6 = \|BK_2\|, \tag{36}$$

Prepared using ocaauth.cls
DOI: 10.1002/oca

$$c_7 = \sup_{t\in[0,T]} e^{-\lambda(T-t)} \int_t^T e^{\lambda\tau} d\tau, \tag{37}$$

$$c_8 = \sup_{t\in[0,T]} e^{-\lambda t} \int_0^t e^{\lambda(T-\tau)} d\tau, \tag{38}$$

where $\tilde{A} = (A - BK_1)$, $\tilde{B} = P$, $K_1 = R^{-1}B^TP$ and $K_2 = R^{-1}B^T$. Based on (1), (2) and (8), it follows that

$$\begin{aligned} d^{n+1}(t) - d^n(t) = (1-k)(d^n(t) - d^{n-1}(t)) + k(f(x_h^n(t), u^n(t)) - f(x_h^{n-1}(t), u^{n-1}(t))) \\ + k((A - BK_1(t))(x_l^{n-1}(t) - x_l^n(t)) + BK_2(r^{n-1}(t) - r^n(t))). \end{aligned}$$

Multiplying both sides of this expression by $e^{-\lambda t}$ and taking the supremum over $[0, T]$ on both sides yields

$$\begin{aligned} \|d^{n+1} - d^n\|_{\lambda_1} \leq \underbrace{|1-k|}_{m_1} \|d^n - d^{n-1}\|_{\lambda_1} + \underbrace{|k|e^{\lambda T}(c_6 + c_5L_2)}_{m_2} \|r^n - r^{n-1}\|_{\lambda_2} \\ + \underbrace{|k|(c_1 + c_4L_2)}_{m_3} \|x_l^n - x_l^{n-1}\|_{\lambda_1} + \underbrace{|k|L_1}_{m_4} \|x_h^n - x_h^{n-1}\|_{\lambda_1}. \end{aligned} \tag{39}$$

The norm of $r^{n+1} - r^n$ is bounded as follows based on (7),

$$\begin{aligned} r^{n+1}(t) - r^n(t) &= \int_t^T \tilde{A}^T[r^{n+1}(\tau) - r^n(\tau)]d\tau + \int_t^T \tilde{B}[d^n(\tau) - d^{n+1}(\tau)]d\tau, \\ \|r^{n+1}(t) - r^n(t)\| &\leq c_2 \int_t^T \|r^{n+1}(\tau) - r^n(\tau)\|d\tau + c_3 \int_t^T \|d^{n+1}(\tau) - d^n(\tau)\|d\tau \\ &\leq c_2\|r^{n+1} - r^n\|_{\lambda_2} \int_t^T e^{\lambda(T-\tau)}d\tau + c_3\|d^{n+1} - d^n\|_{\lambda_1} \int_t^T e^{\lambda\tau}d\tau. \end{aligned}$$

Multiplying by $e^{-\lambda(T-t)}$ and taking the supremum over $[0, T]$ on both sides yields

$$\|r^{n+1} - r^n\|_{\lambda_2} \leq \underbrace{\frac{c_3c_7}{1 - \lambda^{-1}c_2}}_{m_5} \|d^{n+1} - d^n\|_{\lambda_1}. \tag{40}$$

The difference $x_l^{n+1} - x_l^n$ is bounded as follows based on (11)

$$\begin{aligned} x_l^{n+1}(t) - x_l^n(t) &= \int_0^t \tilde{A}(\tau)[x_l^{n+1}(\tau) - x_l^n(\tau)]d\tau + \int_0^t BK_2[r^{n+1}(\tau) - r^n(\tau)]d\tau \\ &\quad + \int_0^t [d^{n+1}(\tau) - d^n(\tau)]d\tau, \\ \|x_l^{n+1}(t) - x_l^n(t)\| &\leq c_1 \int_0^t \|x_l^{n+1}(\tau) - x_l^n(\tau)\|d\tau + c_6 \int_0^t \|r^{n+1}(\tau) - r^n(\tau)\|d\tau \\ &\quad + \int_0^t \|d^{n+1}(\tau) - d^n(\tau)\|d\tau \\ &\leq c_1\|x_l^{n+1} - x_l^n\|_{\lambda_1} \int_0^t e^{\lambda\tau}d\tau + c_6\|r^{n+1} - r^n\|_{\lambda_2} \int_0^t e^{\lambda(T-\tau)}d\tau \end{aligned}$$

DOI: 10.1002/oca

$$+ \|d^{n+1} - d^n\|_{\lambda_1} \int_0^t e^{\lambda\tau} d\tau.$$

Multiplying both sides of the last expression by $e^{-\lambda t}$ and taking the supremum over $[0, T]$ on both sides yields

$$\|x_l^{n+1} - x_l^n\|_{\lambda_1} \leq \underbrace{\frac{\lambda^{-1}}{1 - \lambda^{-1} c_1}}_{m_6} \|d^{n+1} - d^n\|_{\lambda_1} + \underbrace{\frac{c_6 c_8}{1 - \lambda^{-1} c_1}}_{m_7} \|r^{n+1} - r^n\|_{\lambda_2}. \tag{41}$$

Finally, the difference $x_h^{n+1} - x_h^n$ is bounded as follows based on (1) and (5),

$$\begin{aligned}
x_h^{n+1}(t) - x_h^n(t) &= \int_0^t [f(x_h^{n+1}(\tau), u^{n+1}(\tau)) - f(x_h^n(\tau), u^n(\tau))] d\tau, \\
\|x_h^{n+1}(t) - x_h^n(t)\| &\leq L_1 \int_0^t \|x_h^{n+1}(\tau) - x_h^n(\tau)\| d\tau + L_2 \int_0^t \|u^{n+1}(\tau) - u^n(\tau)\| d\tau \\
&\leq L_1 \int_0^t \|x_h^{n+1}(\tau) - x_h^n(\tau)\| d\tau + c_4 L_2 \int_0^t \|x_l^{n+1}(\tau) - x_l^n(\tau)\| d\tau \\
&\quad + c_5 L_2 \int_0^t \|r^{n+1}(\tau) - r^n(\tau)\| d\tau \\
&\leq L_1 \|x_h^{n+1} - x_h^n\|_{\lambda_1} \int_0^t e^{\lambda\tau} d\tau + c_4 L_2 \|x_l^{n+1} - x_l^n\|_{\lambda_1} \int_0^t e^{\lambda\tau} d\tau \\
&\quad + c_5 L_2 \|r^{n+1} - r^n\|_{\lambda_2} \int_0^t e^{\lambda(T-\tau)} d\tau.
\end{aligned}$$

Multiplying the last expression by $e^{-\lambda t}$ and taking the supremum over $[0, T]$ on both sides yields

$$\|x_h^{n+1} - x_h^n\|_{\lambda_1} \leq \underbrace{\frac{c_5 c_8 L_2}{1 - \lambda^{-1} L_1}}_{m_8} \|r^{n+1} - r^n\|_{\lambda_2} + \underbrace{\frac{\lambda^{-1} c_4 L_2}{1 - \lambda^{-1} L_1}}_{m_9} \|x_l^{n+1} - x_l^n\|_{\lambda_1}. \tag{42}$$

Using (40)-(42), (39) can be written in the same form as (19),

$$\|d^{n+1} - d^n\|_{\lambda_1} \leq \alpha \|d^n - d^{n-1}\|_{\lambda_1}, \tag{43}$$

where

$$\alpha = m_1 + m_2 m_5 + m_3(m_6 + m_5 m_7) + m_4(m_5 m_8 + (m_6 + m_5 m_7) m_9). \tag{44}$$

APPENDIX B: PROOF OF PROPOSITION 1

Using (43), the following inequality is obtained for $m, n \in \mathbb{N}$ and $m > n$,

$$\begin{aligned}
\|d^m - d^n\|_{\lambda_1} &\leq \|d^m - d^{m-1}\|_{\lambda_1} + \|d^{m-1} - d^{m-2}\|_{\lambda_1} + \ldots + \|d^{n+1} - d^n\|_{\lambda_1} \\
&\leq \alpha^{m-1} \|d^1 - d^0\|_{\lambda_1} + \alpha^{m-2} \|d^1 - d^0\|_{\lambda_1} + \ldots + \alpha^n \|d^1 - d^0\|_{\lambda_1}
\end{aligned}$$

Prepared using ocaauth.cls
DOI: 10.1002/oca

$$
\begin{aligned}
&= \|d^1 - d^0\|_{\lambda_1} \alpha^n \sum_{k=0}^{m-n-1} \alpha^k \\
&\leq \|d^1 - d^0\|_{\lambda_1} \alpha^n \sum_{k=0}^{\infty} \alpha^k \\
&= \|d^1 - d^0\|_{\lambda_1} \frac{\alpha^n}{(1-\alpha)}.
\end{aligned}
$$

If $\alpha \in (0,1)$, then for all $\epsilon > 0$, there exists $N \in \mathbb{N}$ such that for all m, $n > N$, $\|d^m - d^n\|_{\lambda_1} < \epsilon$, where $N \in \mathbb{N}$ can be chosen such that $\alpha^N < \frac{\epsilon(1-\alpha)}{\|d^1 - d^0\|_{\lambda_1}}$. This shows that $\{d^n\}_{n=0}^{\infty}$ is a Cauchy sequence of continuous functions in $C^0([0,T])$, which is a complete normed linear space under $\|\cdot\|_{\lambda_1}$. Hence $\lim_{n\to\infty} d^n = d^\infty$ for some d^∞ uniformly on $[0,T]$.

Using (40), (41) and (42) it follows similarly that $\{r^n\}_{n=0}^{\infty}$ $\{x_l^n\}_{n=0}^{\infty}$ and $\{x_h^n\}_{n=0}^{\infty}$ are Cauchy sequences of continuous functions in $C^0([0,T])$, and hence $\lim_{n\to\infty} r^n = r^\infty$, $\lim_{n\to\infty} x_l^n = x_l^\infty$ and $\lim_{n\to\infty} x_h^n = x_h^\infty$ uniformly on $[0,T]$ for appropriate continuous functions r^∞, x_l^∞ and x_h^∞, respectively. As an example, for r^n, we have

$$
\begin{aligned}
\|r^m - r^n\|_{\lambda_2} &\leq \|r^m - r^{m-1}\|_{\lambda_2} + \|r^{m-1} - r^{m-2}\|_{\lambda_2} + \ldots + \|r^{n+1} - r^n\|_{\lambda_2} \\
&\leq m_5(\|d^m - d^{m-1}\|_{\lambda_1} + \|d^{m-1} - d^{m-2}\|_{\lambda_1} + \ldots + \|d^{n+1} - d^n\|_{\lambda_1}) \\
&\leq \frac{m_5}{1-\alpha}(\alpha^{m-1}\|d^1 - d^0\|_{\lambda_1} + \alpha^{m-2}\|d^1 - d^0\|_{\lambda_1} + \ldots + \alpha^n\|d^1 - d^0\|_{\lambda_1}) \\
&= \|d^1 - d^0\|_{\lambda_1} \frac{m_5\alpha^n}{1-\alpha} \sum_{k=0}^{m-n-1} \alpha^k \\
&\leq \|d^1 - d^0\|_{\lambda_1} \frac{m_5\alpha^n}{1-\alpha} \sum_{k=0}^{\infty} \alpha^k \\
&= \|d^1 - d^0\|_{\lambda_1} \frac{m_5\alpha^n}{(1-\alpha)^2},
\end{aligned}
$$

where m, $n \in \mathbb{N}$ and $m > n$. Now, if $\alpha \in (0,1)$, then for all $\epsilon > 0$, there exists $N \in \mathbb{N}$ such that for all m, $n > N$, it implies $\|r^m - r^n\|_{\lambda_2} < \epsilon$, where $N \in \mathbb{N}$ can be chosen such that $\alpha^N < \frac{\epsilon(1-\alpha)^2}{\|d^1 - d^0\|_{\lambda_1} m_5}$.

From (8),

$$
\|\dot{e}^n\|_{\lambda_1} = \frac{\|d^n - d^{n-1}\|_{\lambda_1}}{|k|},
$$

and $\lim_{n\to\infty} \|\dot{e}^n\|_\infty = 0$. Since $e^n(0) = 0$,

$$
\|e^n\|_\infty = \sup_{t\in[0,T]} \left\| \int_0^t \dot{e}^n(\tau) d\tau \right\| \leq \|\dot{e}^n\|_\infty T.
$$

Thus

$$
\lim_{n\to\infty} \|e^n\|_\infty = \lim_{n\to\infty} \|x_h^n - x_l^n\|_\infty = 0,
$$

and $x_h^\infty = x_l^\infty$.

Prepared using ocaauth.cls
DOI: 10.1002/oca

Using uniform convergence of sequences and passing to the limit, $J_l^\infty = \lim_{n\to\infty} J_l(x_l^n, u^n) = J_l(\lim_{n\to\infty} x_l^n, \lim_{n\to\infty} u^n) = J_l(x_l^\infty, u^\infty) = J_h(x_h^\infty, u^\infty) = J_h(\lim_{n\to\infty} x_h^n, \lim_{n\to\infty} u^n) = \lim_{n\to\infty} J_h(x_h^n, u^n) = J_h^\infty$. This completes the proof.

APPENDIX C: COMPUTATION OF (20)

We have

$$
\begin{aligned}
&K_1 = R^{-1}B^T P = 0.05P,\\
&K_2 = R^{-1}B^T = 0.05,\\
&\tilde{A} = (A - BK_1) = -0.1 - 0.0025P,\\
&\tilde{B} = P.
\end{aligned}
$$

The P in (6) satisfies

$$
\begin{aligned}
&\dot{P} = 0.2P + 0.0025P^2 - 1,\\
&P(2) = 10.
\end{aligned}
$$

We can express P as an explicit function of t by separation of variables,

$$
P(t) = \frac{40\sqrt{5}}{1 - \exp\left(\frac{\sqrt{5}}{10}(t-2) + \ln(\frac{50-20\sqrt{5}}{50+20\sqrt{5}})\right)} - 40 - 20\sqrt{5},
$$

and it is an increasing function of $t \in [0, T]$.

According to (31)-(38),

$$
\begin{aligned}
c_1 &= \sup_{t\in[0,T]} \|\tilde{A}(t)\| = \sup|0.1 + 0.0025P| = 0.125,\\
c_2 &= \sup_{t\in[0,T]} \|\tilde{A}^T(t)\| = \sup|0.1 + 0.0025P| = 0.125,\\
c_3 &= \sup_{t\in[0,T]} \|\tilde{B}(t)\| = \sup|P| = 10,\\
c_4 &= \sup_{t\in[0,T]} \|K_1(t)\| = \sup|0.05P| = 0.5,\\
c_5 &= \|K_2\| = 0.05,\\
c_6 &= \|BK_2\| = 0.0025,\\
c_7 &= \sup_{t\in[0,T]} e^{-\lambda(T-t)} \int_t^T e^{\lambda\tau} d\tau = 1.3834,\\
c_8 &= \sup_{t\in[0,T]} e^{-\lambda t} \int_0^t e^{\lambda(T-\tau)} d\tau = 1.3834.
\end{aligned}
$$

DOI: 10.1002/oca

Then, according to (39)-(42),

$$
\begin{aligned}
m_1 &= |1-k| = 0.9,\\
m_2 &= |k|e^{\lambda T}(c_6 + c_5 L_2) = 0.0017,\\
m_3 &= |k|(c_1 + c_4 L_2) = 0.015,\\
m_4 &= |k|L_1 = 0.01,\\
m_5 &= \frac{c_3 c_7}{1-\lambda^{-1}c_2} = 17.4742,\\
m_6 &= \frac{\lambda^{-1}}{1-\lambda^{-1}c_1} = 2.1053,\\
m_7 &= \frac{c_6 c_8}{1-\lambda^{-1}c_1} = 0.0044,\\
m_8 &= \frac{c_5 c_8 L_2}{1-\lambda^{-1}L_1} = 0.0042,\\
m_9 &= \frac{\lambda^{-1}c_4 L_2}{1-\lambda^{-1}L_1} = 0.05,
\end{aligned}
$$

where $L_1 = 0.1$ and $L_2 = 0.05$ are the Lipschitz constants of the high-fidelity model. Finally,

$$\alpha = m_1 + m_2 m_5 + m_3(m_6 + m_5 m_7) + m_4(m_5 m_8 + (m_6 + m_5 m_7)m_9) = 0.9635.$$

APPENDIX D: PROOF OF PROPOSITION 2

Let u^* denote an optimal control for the high-fidelity model and x^* denote the corresponding state trajectory. Let $J^* = J(x^*, u^*)$ denote the corresponding cost where $J(x,u)$ is defined by (3). Consider the system,

$$\dot{x} = Ax + Bu + d^*(t), \tag{45}$$

obtained by evaluating $d_h(x,t)$ of (21) at x^*, i.e., $d^*(t) = d_h(x^*(t), t)$. Note that the control and state pair (u^*, x^*) represents one trajectory of (45), such that the integration of

$$\dot{x} = Ax + Bu^* + d^*(t), \quad x(0) = x^*(0), \tag{46}$$

recovers the optimal trajectory x^* of the high-fidelity model. For the same cost function $J(x,u)$, the system (45) has a unique optimal control-state pair (u°, x°), satisfying

$$\dot{x}^\circ = Ax^\circ + Bu^\circ + d^*(t), \tag{47}$$

and let the corresponding cost be J°. Since (u°, x°) is optimal for (45),

$$J^\circ \leq J^*. \tag{48}$$

Prepared using ocaauth.cls
DOI: 10.1002/oca

Suppose the IMTR iterations converge and denote the corresponding control-state pair by $(\tilde{u}, \tilde{x})$. Then,

$$\begin{aligned} \dot{\tilde{x}} &= A\tilde{x} + B\tilde{u} + d_h(\tilde{x}(t), t), \\ \dot{\tilde{x}} &= A\tilde{x} + B\tilde{u} + d_l(t), \end{aligned} \tag{49}$$

where

$$d_l(t) = d_h(\tilde{x}(t), t). \tag{50}$$

By (22), (50) and the triangular inequality, we have,

$$\begin{aligned} \|d^*(t) - d_l(t)\| &= \|d_h(x^*(t), t) - d_h(\tilde{x}(t), t)\| \\ &= \|d_h(x^*(t), t) - \bar{d}(t) + \bar{d}(t) - d_h(\tilde{x}(t), t)\| \\ &\leq \|d_h(x^*(t), t) - \bar{d}(t)\| + \|d_h(\tilde{x}(t), t) - \bar{d}(t)\| \\ &\leq 2\epsilon. \end{aligned} \tag{51}$$

Note that,

$$\begin{aligned} u^\circ &= -R^{-1}B^T P(t)x^\circ + R^{-1}B^T r^\circ, \\ \tilde{u} &= -R^{-1}B^T P(t)\tilde{x} + R^{-1}B^T \tilde{r}, \end{aligned} \tag{52}$$

where $P(t)$ comes from (6) and is the same in both cases, and

$$\begin{aligned} \dot{r}^\circ &= \bar{A}(t)r^\circ + \bar{B}(t)d^*(t), \\ \dot{\tilde{r}} &= \bar{A}(t)\tilde{r} + \bar{B}(t)d_l(t), \end{aligned}$$

where $\bar{A}(t) = -(A - BR^{-1}B^T P(t))^T$ and $\bar{B}(t) = P(t)$. We evaluate the system (47) and (49) with the feedback control (52), and

$$\begin{aligned} \dot{x}^\circ &= \tilde{A}(t)x^\circ + \tilde{B}(t)r^\circ + d^*(t), \\ \dot{\tilde{x}} &= \tilde{A}(t)\tilde{x} + \tilde{B}(t)\tilde{r} + d_l(t), \end{aligned}$$

where $\tilde{A}(t) = (A - BR^{-1}B^T P(t))$ and $\tilde{B}(t) = BR^{-1}B^T$. Note that $x^\circ(0) = \tilde{x}(0)$ and $r^\circ(T) = \tilde{r}(T)$. Let $\Delta x = x^\circ - \tilde{x}$, $\Delta r = r^\circ - \tilde{r}$ and $\Delta d(t) = d^*(t) - d_l(t)$. Then,

$$\begin{bmatrix} \Delta\dot{x} \\ \Delta\dot{r} \end{bmatrix} = \begin{bmatrix} \tilde{A}(t) & \tilde{B}(t) \\ 0 & \bar{A}(t) \end{bmatrix} \begin{bmatrix} \Delta x \\ \Delta r \end{bmatrix} + \begin{bmatrix} I \\ \bar{B}(t) \end{bmatrix} \Delta d, \tag{53}$$

where the input Δd is bounded by $\|\Delta d(t)\| \leq 2\epsilon$ for all $t \in [0, T]$, $\Delta x(0) = 0$ and $\Delta r(T) = 0$. From (53),

$$\begin{aligned} \Delta r(t) &= \Phi(t, T)\Delta r(T) + \int_T^t \Phi(t, \tau)\bar{B}(\tau)\Delta d(\tau)\, d\tau \\ &= \int_T^t \Phi(t, \tau)\bar{B}(\tau)\Delta d(\tau)\, d\tau, \end{aligned}$$

Prepared using ocaauth.cls
DOI: 10.1002/oca

where $\Phi(t,\tau)$ is the state transition matrix associated with $\bar{A}(t)$. Hence

$$\begin{aligned}\|\Delta r(t)\| &= \left\| \int_T^t \Phi(t,\tau)\bar{B}(\tau)\Delta d(\tau)\, d\tau \right\| \\ &\leq \int_t^T \|\Phi(t,\tau)\bar{B}(\tau)\Delta d(\tau)\|\, d\tau \\ &\leq 2\epsilon(T-t)C_1(t), \end{aligned} \tag{54}$$

where $C_1(t) = \|\Phi(t,\tau)\bar{B}(\tau)\|_\infty$ and $\|\cdot\|_\infty$ is the supremum of $\|\cdot\|$ over $\tau \in [t,T]$. Note that $C_1(t)$ can be chosen to be finite and independent of ϵ. Thus, $\|\Delta r(t)\|$ is $O(\epsilon)$.

Similarly, from (53) and $\Delta x(0) = 0$,

$$\Delta x(t) = \int_0^t \Psi(t,\tau)(\tilde{B}(\tau)\Delta r(\tau) + \Delta d(\tau))\, d\tau,$$

where $\Psi(t,\tau)$ is the state transition matrix associated with $\tilde{A}(t)$. Using (54), it follows that

$$\|\Delta x(t)\| \leq 2\epsilon t C_2(t), \tag{55}$$

where $C_2(t) = \|\Psi(t,\tau)\tilde{B}(\tau)\|_\infty \|(T-\tau)C_1(\tau)\|_\infty + \|\Psi(t,\tau)\|_\infty$ and $\|\cdot\|_\infty$ is the supremum of $\|\cdot\|$ over $\tau \in [0,t]$. Note that $C_2(t)$ can be chosen to be finite and independent of ϵ. Thus, $\|\Delta x(t)\|$ is $O(\epsilon)$.

Similarly, from (52)

$$\|\Delta u(t)\| \leq C_3(t)\|\Delta x\| + C_4\|\Delta r\|, \tag{56}$$

where

$$\begin{aligned} C_3(t) &= \|R^{-1}B^T P(t)\|, \\ C_4 &= \|R^{-1}B^T\|, \end{aligned}$$

are independent from ϵ and are bounded.

Finally, the Taylor expansion of $\tilde{J}$ about the trajectory of (u°, x°) gives

$$\begin{aligned}\tilde{J} &= \frac{1}{2}\tilde{x}(T)^T K_f \tilde{x}(T) + \frac{1}{2}\int_0^T [\tilde{x}(t)^T Q\tilde{x}(t) + \tilde{u}(t)^T R\tilde{u}(t)]dt \\ &= J^\circ - x^\circ(T)^T K_f \Delta x(T) - \int_0^T [x^\circ(t)^T Q\Delta x(t) + u^\circ(t)^T R\Delta u(t)]dt + O(\epsilon^2). \end{aligned}$$

Therefore, based on (54), (55) and (56), the difference between J° and $\tilde{J}$ is $O(\epsilon)$.

In particular, because $(\tilde{u}, \tilde{x})$ is one control-state pair of trajectories of the high-fidelity model while (u^*, x^*) is the optimal control-state pair of trajectories,

$$J^* \leq \tilde{J}. \tag{57}$$

Based on (48) and (57), we have

$$J^\circ \leq J^* \leq \tilde{J},$$

Prepared using ocaauth.cls
DOI: 10.1002/oca

and thus

$$|\tilde{J} - J^*| \leq |\tilde{J} - J^\circ|.$$

Thus, $|\tilde{J} - J^*|$ is $O(\epsilon)$ and the proof is complete.

DOI: 10.1002/oca